AD-A137 777 TUNABLE FAR INFRARED SEMICONDUCTOR SOURCES(U) INNSBRUCK 1/1
UNIV (AUSTRIA) INST OF EXPERIMENTAL PHYSICS E GORNIK
JAN 84 DAJA37-81-C-0046

UNCLASSIFIED F/G 20/2 NL

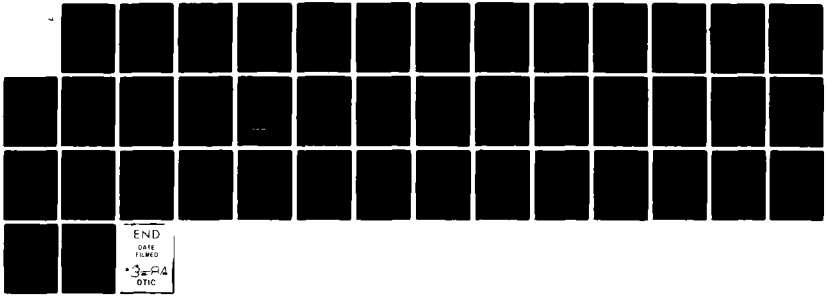

END
DATE FILMED
3-84
DTIC

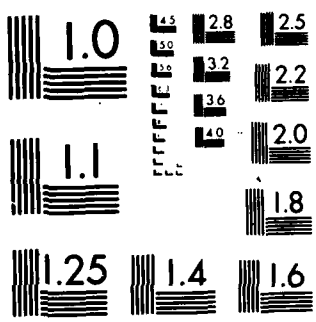

UNCLASSIFIED

SECURITY CLASSIFICATION OF THIS PAGE (When Data Entered)

R&D 2642-EE

REPORT DOCUMENTATION PAGE		READ INSTRUCTIONS BEFORE COMPLETING FORM
1. REPORT NUMBER	2. GOVT ACCESSION NO. AD-A137777	3. RECIPIENT'S CATALOG NUMBER
4. TITLE (and Subtitle) Tunable Far Infrared Semiconductor Sources		5. TYPE OF REPORT & PERIOD COVERED Final Technical Report Oct 80 - Jan 84
		6. PERFORMING ORG. REPORT NUMBER
7. AUTHOR(s) Prof. Dr. Erich Gornik		8. CONTRACT OR GRANT NUMBER(s) DAJA 37-81-C-0046
9. PERFORMING ORGANIZATION NAME AND ADDRESS Institut für Experimentalphysik Innsbruck, Austria		10. PROGRAM ELEMENT, PROJECT, TASK AREA & WORK UNIT NUMBERS 6.11.02A 1T161102BH57-03
11. CONTROLLING OFFICE NAME AND ADDRESS USARDSG-UK Box 65, FPO NY 09510		12. REPORT DATE Jan 84
		13. NUMBER OF PAGES 37
14. MONITORING AGENCY NAME & ADDRESS (if different from Controlling Office)		15. SECURITY CLASS. (of this report) Unclassified
		15a. DECLASSIFICATION/DOWNGRADING SCHEDULE

AD A137777

16. DISTRIBUTION STATEMENT (of this Report)

Approved for Public Release; distribution unlimited

17. DISTRIBUTION STATEMENT (of the abstract entered in Block 20, if different from Report)

18. SUPPLEMENTARY NOTES

19. KEY WORDS (Continue on reverse side if necessary and identify by block number)

tunable far infrared sources
far infrared spectroscopy
2-dimensional plasmons in Si-MOS
hot electron transport in Si-MOS-devices

20. ABSTRACT (Continue on reverse side if necessary and identify by block number)

The concept of continuously tunable far infrared sources was investigated in magnetically and electrically tunable level systems. Landau emission has been investigated in several semiconductors. A useful source for spectroscopic investigations based on bulk GaAs with a resolution below 1 cm^{-1} has been developed in the spectral range 20 - 120 cm^{-1}. New promising concepts for tunable sources have been demonstrated recently: A significant line narrowing of the Landau emission was observed from InSb under the presence of hydrostatic

DD FORM 1 JAN 73 1473 EDITION OF 1 NOV 65 IS OBSOLETE

UNCLASSIFIED

SECURITY CLASSIFICATION OF THIS PAGE (When Data Entered)

20. pressure above 8 kbar. For the first time tunable emission from spin-flip transitions in uniaxially stressed InSb was observed. Linewidths in the order of 0.2 cm^{-1} are found which opens the potential for high resolution spectroscopy with magnetically tunable sources.
For the realization of voltage tunable sources based on the voltage tunable electron density in MOS-devices, three possible mechanisms were investigated: The radiative recombination between electric subbands, between minigaps induced by tilted interfaces in respect to the main cristallographic directions and the radiative decay of two-dimensional plasma-oscillations via periodic grating structures.
The only promising system for an application is the so called plasmon-emission, which was investigated in detail. The theoretical and experimental work could clear up the mechanisms of plasmon excitation as a thermal process resulting from the different scattering mechanisms of the heated electron system. The emission experiments can be quantitatively explained by the model of plasmon excitation in thermal equilibrium.
The possibility of coherent plasmon emission is discussed and an experimental realization is predicted in the system GaAs/GaAlAs.

"TUNABLE FAR INFRARED SEMICONDUCTOR SOURCES"

Principal investigator and contractor

Prof. Dr. Erich Gornik
Institut für Experimentalphysik
Schöpfstraße 41
A-6020 Innsbruck
AUSTRIA

Contract Number: DAJA 37-81-C-0046

final technical report

22 October 1980 - 31 December 1983

"The research reported in this document has been made possible through the support and sponsorship of the U.S.Government through its U.S. Army Research and Standardisation Group (Europe). This report is intended only for the internal management use of the contractor and the U.S. Government".

List of publications

(published with partial support of project DAJA 37-81-C-0046)

E. Gornik, "Application of High Magnetic Fields in Semiconductor Physics", Lecture Notes in Physics Vol. 177, ed. by G. Landwehr (1983) 248-258 (invited paper).

R.A. Höpfel, G. Lindemann, E. Gornik, G. Stangl, A.C. Gossard, W. Wiegmann, Surface Sci. 113 (1982) 118.

R.A. Höpfel, E. Vass, E. Gornik, Phys.Rev.Lett. 49 (1982) 1667.

E. Gornik, R.A. Höpfel, AEÜ Electronics and Communication 37 (1983) 213.

R.A. Höpfel, E. Gornik, A.C. Gossard, W. Wiegmann, Proc. 16th Int.Conf. on "The Physics of Semicond.", Montpellier, France 1982, ed. by M. Averous (North Holland, Amsterdam 1983) p. 646.

R.A. Höpfel, E. Gornik, "Two-Dimensional Plasmons and Infrared Emission", Invited paper at the 5th Int.Conf. on "Electronic Properties of Two-Dimensional Systems", Oxford, U.K. 1983, Proceedings in Surface Science (1984, in press).

"TUNABLE FAR INFRARED SEMICONDUCTOR SOURCES"

E. Gornik and R.A. Höpfel

Contents

A) MAGNETICALLY TUNABLE SOURCES

Summary

Landau emission has been investigated in several semiconductors. A useful source for spectroscopic investigations based on bulk GaAs with a resolution below 1 cm^{-1} has been developed in the spectral range 20 - 120 cm^{-1}. New promising concepts for tunable sources have been demonstrated recently: A significant line narrowing of the Landau emission was observed from InSb under the presence of hydrostatic pressure above 8 kbar. For the first time tunable emission from spin-flip transitions in uniaxially stressed InSb was observed. Linewidths in the order of 0.2 cm^{-1} are found which opens the potential for high resolution spectroscopy with magnetically tunable sources.

A.1. LANDAU EMISSION

Tunable emission between Landau levels has been observed in several semiconductors /1/. A detailed study of the emission spectrum excited by electrical current heating has been performed in InSb and GaAs. From a source aspect GaAs turns out to be the more favourable candidate since linewidths below 1 cm^{-1} and intensities comparable with those in InSb in the order of 10^{-8} to 10^{-7} W/cm^2cm^{-1} have been achieved.

A typical emission spectrum with a resolution of 0.25 cm^{-1} from a high purity GaAs sample for different bias electric fields is shown in figure 1. The spectrum is obtained by tuning the emission line through one of the narrow lines of the GaAs detector in a magnetic field. At low electric fields (below 15 V/cm) the spectrum consists only of one narrow line due to transitions between the n = 1 and the n = 0 Landau levels.

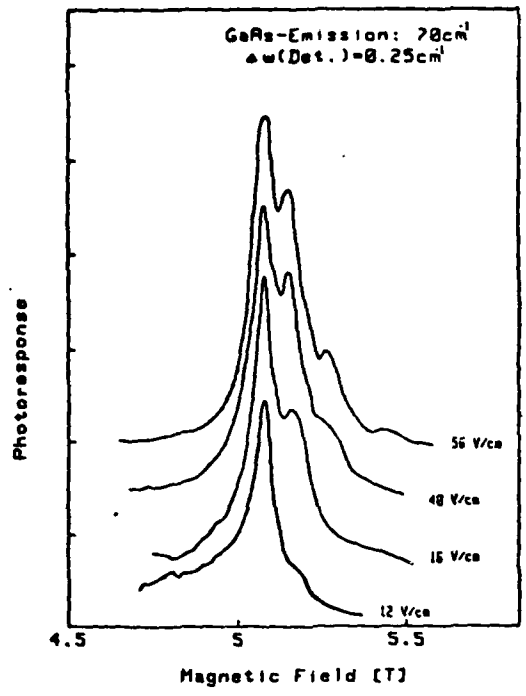

Fig. 1: Emission spectrum of a high purity GaAs emitter as a function of magnetic field for several bias electric fields as observed with a GaAs detector.

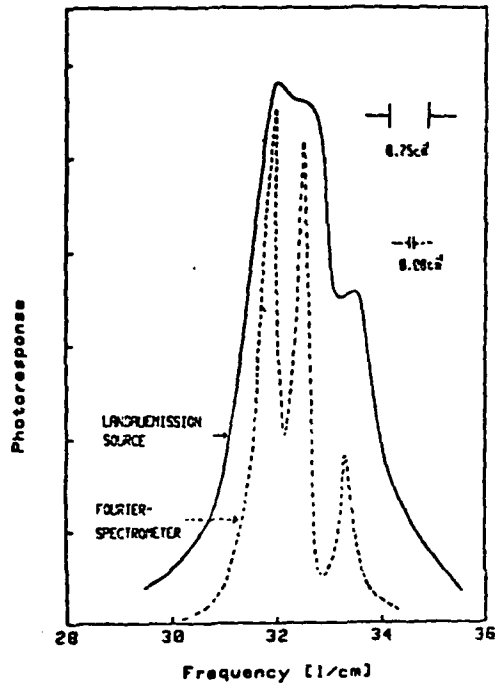

Fig. 2: Photoconductive spectrum of the lowest impurity line (see fig. 2) of a GaAs sample (doping level $N_I \sim 3x10^{14}cm^{-3}$) as obtained with a narrowband GaAs Landau source and a Fourier Spectrometer.

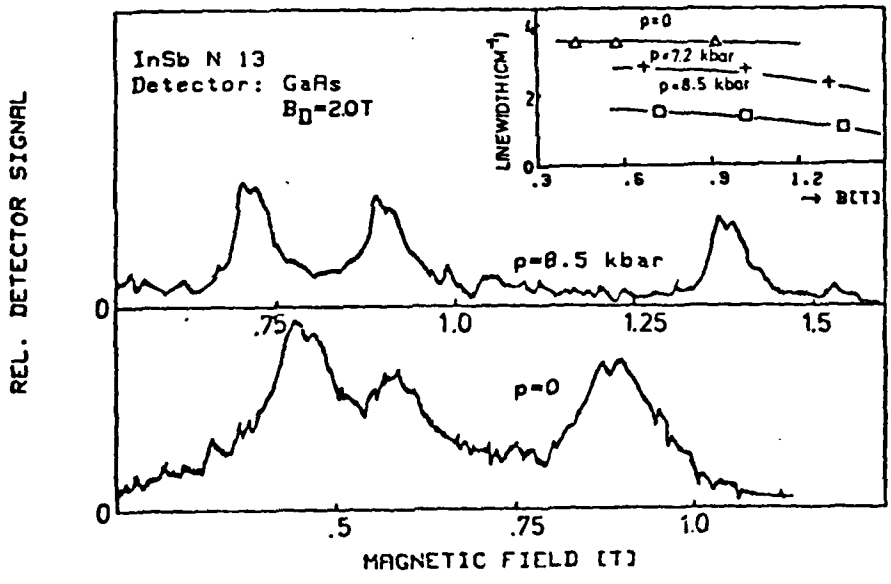

Fig. 3: Landau emission spectra of an n-InSb-sample (doping level $N_I \sim 5x10^{14}cm^{-3}$, $n=8x10^{13}$ cm^{-3}) as a function of magnetic field detected with a GaAs detector at 2.0 T. The applied hydrostatic pressure is indicated. The insert shows the obtained linewidth.

With increasing field additional lines due to transitions between higher levels (n = 2 to n = 1, n = 3 to n = 2) appear. The splitting of the lines is a consequence of nonparabolicity and polaron effects as it has been demonstrated by Lindemann et al. /2/. For source applications only the spectrum with the single line (lowest field) can be used which limits the usable intensities to a factor of 5 below the maximum values.

An example of a spectroscopic application with a tunable GaAs-source with a linewidth of 0.75 cm^{-1} is shown in figure 2. The photoresponse of a GaAs sample at 32 cm^{-1} in a magnetic field is plotted in comparison with the result of an analysis with a high resolution Fourier Transform Spectrometer (FTS). The 3 apparent lines are due to central cell splittings of different shallow impurity species /3/. The lines are well-resolved with the FTS and at the edge of resolution with the GaAs source.

However this example demonstrates that Landau emission sources can be used for spectroscopy with resolution down to 1 cm^{-1}. Especially in the area of detector testing they provide a very practical tool. In addition, the fact that the linewidth is proportional to the square root of the total ionized impurity content enables the determination of doping levels by analysing the emission spectrum, which is of significant interest for material growth /4/.

A.2. InSb WITH HYDROSTATIC PRESSURE

New impact has come to the field by the application of hydrostatic pressure to n-InSb /5/. From conductivity and photoresponse measurements it was found that the active ionized impurity concentration can be reduced above certain pressure levels. As a consequence a line narrowing for Landau emission is expected. An emission experiment performed for different values of hydrostatic pressure is shown in figure 3 /6/. The photosignal of a GaAs detector at 2.0T is plotted as a func-

tion of the InSb emitter magnetic field. The positions of the detector lines in terms of frequencies can be found from figure 4 by drawing a horizontal line at 2.0T. The emission spectrum consists of two lines due to transitions between the two lowest Landau levels for different spin orientations. The individual linewidth is determined by a curve fitting procedure. The result is shown in the insert of figure 3. A drastic line-narrowing with increasing pressure by about a factor of two is observed. This demonstrates that the source properties of InSb can be improved. It is interesting to note that the obtained linewidth is lowered to values which cannot be explained with the residual shallow impurities. This means that the dominant impurity scattering process must be changed with pressure.

A.3. SPIN FLIP EMISSION FROM UNIAXIALLY STRESSED InSb

Under certain circumstances spin resonance (SR) transitions, which involve a change in the spin state of the electrons (spin flip) can be excited by electric dipol radiation. The matrix elements of these in principle forbidden transitions are increased by two reasons: 1. A mixing of electronic states by the interaction of different energy bands especially important in narrow gap semiconductors /7/.
2. The lack of inversion symmetry /8/. In the presence of uniaxial stress the inversion asymmetry is increased leading to a strong mixing of different spin states connected with a strong enhancement of the matrix elements /9/.

In narrow gap semiconductors without uniaxial stress the first mechanism dominates /10/ and combined resonances and SR resonances have been investigated in detail in HgCdTe /11/ and InSb /10,12,13/. Three narrow lines were observed in SR experiments in InSb. The central line could be identified

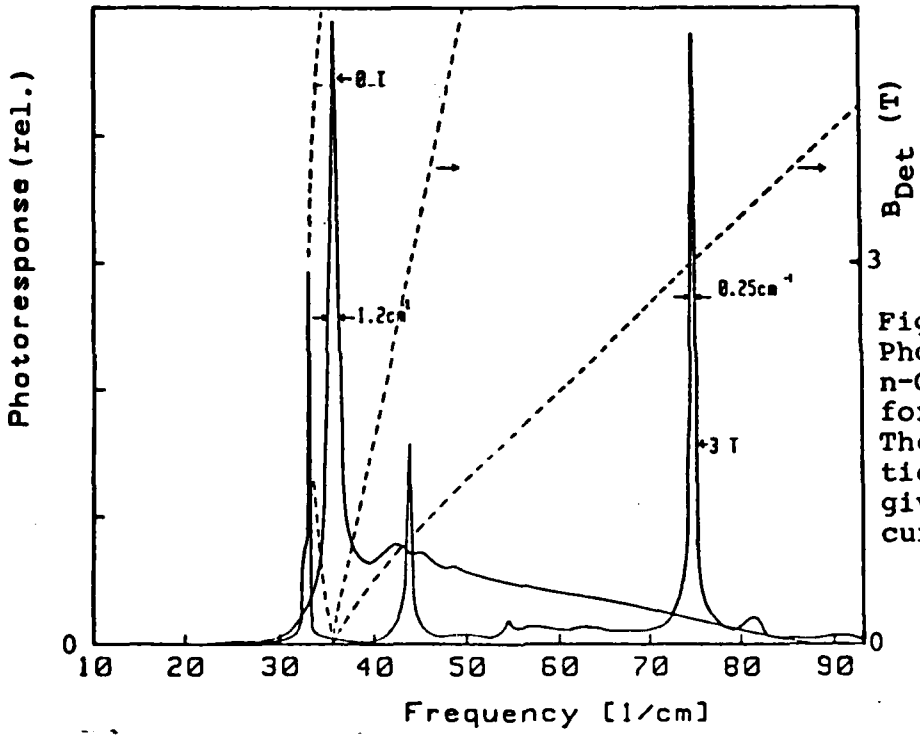

Fig. 4:
Photoresponse of a n-GaAs detector at 4.2K for OT and 3.0 T. The tuning characteristic of the three lines is given by the dashed curves.

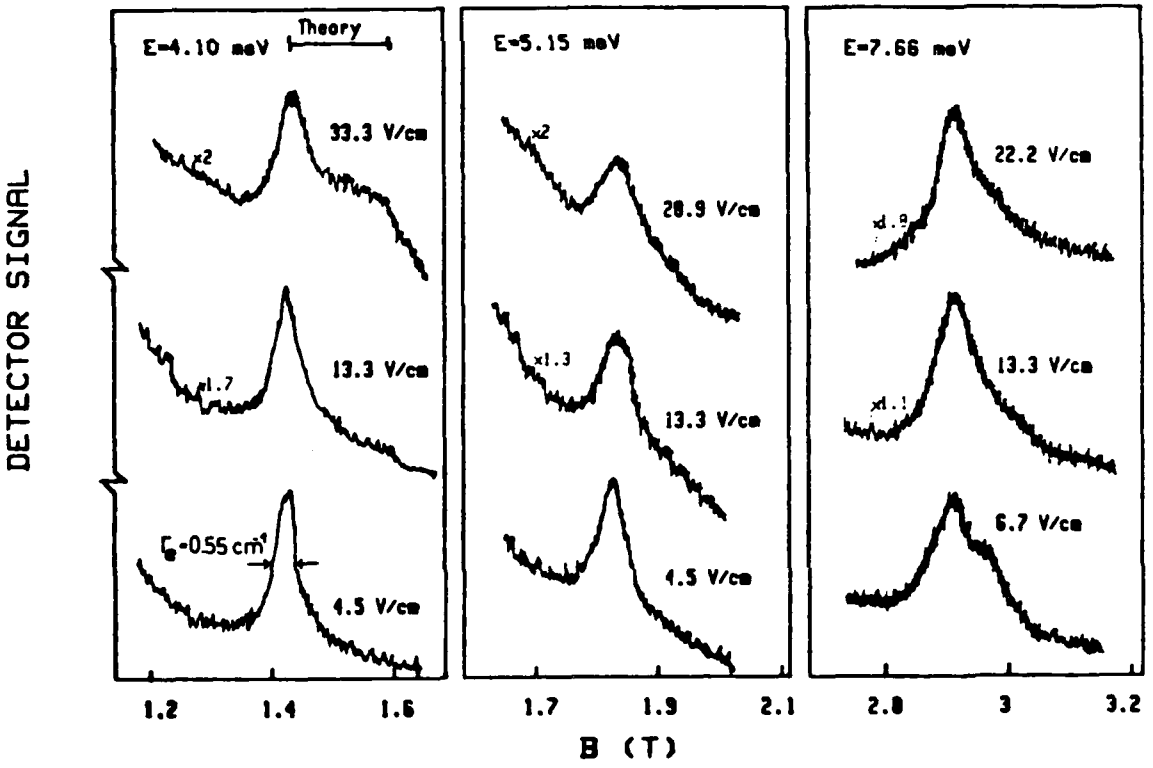

Fig. 5: Experimentally observed emission spectra for three different resonance energies of a narrowband detector line. All intensities are normalized and the electric field applied to the InSb sample is given. The indicated bar represents calculations of the magnetic field difference of $(0^- - 0^+)$ and $(1^- - 1^+)$ transitions.

as the free-carrier SR transition, the other lines as SR transitions involving electrons localized at impurities. The corresponding impurity transition could not be assigned unambiguously up to now.

Uniaxial stress was shown to enhance the matrix elements for SR transitions due to a reduction of symmetry by several orders of magnitude. A strong increase of the photoconductivity signal with uniaxial stress || [110] was demonstrated and explained in terms of a sixband model /9/. In the following this work was extended to other crystallographic directions and coupling parameters for the matrix elements were determined /14,15/.

The enhancement of the matrixelement due to uniaxial stress provides the basis for the observation and the analysis of SR emission spectra. The emitted radiation is analyzed in the wavenumber range between 33 and 70 cm^{-1} with a resolution of 0.25 cm^{-1} using a GaAs detector in a magnetic field. SR emission intensities are determined from a comparison with CR emission intensities and the emission linewidth is measured as a function of frequency and applied electric field. In addition to the free electron SR transitions ($0^- - 0^+$) SR transitions connected with the first Landau level were observed.

The InSb sample was glued at two opposite points on a brass ring. The uniaxial stress is simply applied due to the different thermal expansion coefficients of InSb and brass when the sample is immersed in liquid He /16/. The stress is estimated to amount about 4 Kbar. The orientation of the sample was [110] in stress direction and [112] parallel to the magnetic field. The characteristics of the InSb sample used in this investigations are: $n = 1 \times 10^{14} cm^{-3}$, $\mu = 6.5 \times 10^5 cm^2/Vs$. Voltage pulses are applied to the emitter and electrons are heated up to occupy high energy states.

Characteristic emission spectra at three different resonant energies of the detector are shown in figure 5. The individual spectra at a certain frequency differ in the applied electric field which is indicated for each spectrum. All curves are normalized and the corresponding factors are given. The absolute intensity is determined by a comparison of the SR emission signal with the well known CR emission signal at a frequency of 36 cm^{-1}. The ratio of the spectral intensity between CR emission and SR emission amounts approximately 40 yielding an absolute spectral intensity of a few times of $10^{-8} W/cm^2 cm^{-1}$. The emission intensity depends on the number of electrons in the 0^- Landau level, which decreases with increasing magnetic field for a given electron distribution. This reduction of the emission intensity as well as the decrease in the detector sensitivity with increasing energy limits the spectral region of the investigations to energies smaller than 9 meV. The low energy limit of the investigations is determined by the lack of an appropriate narrowband detector line at energies smaller than 4.1 meV.

Summarizing, narrowband FIR emission has been observed and analysed in uniaxial stressed InSb and has been explained by spin flip emission. The features of this radiation are an extremely small linewidth and a weak intensity which can be still improved to our opinion. An application of this FIR emission as a source for high resolution spectroscopy seems possible.

Landau emission has been and still is a candidate of attention for a narrowband tunable and coherent source. Some concepts including resonant 2 photon pumping across the gap and tunnel injection have not been tried extensively. A mechanism which predicts population inversion by electrical exitation is the streaming motion of carriers in crossed fields /17/.

B) VOLTAGE TUNABLE SOURCES

Summary

For the realization of voltage tunable sources based on the voltage tunable electron density in MOS-devices, three possible mechanisms were investigated: The radiative recombination between electric subbands, between minigaps induced by tilted interfaces in respect to the main cristallographic directions and the radiative decay of two-dimensional plasma-oscillations via periodic grating structures.

The radiative recombination between electric subbands /18/ is limited in the total intensity to about 10^{-11}W, since the radiation is emitted parallel to the Si/SiO_2-interface which results in a small effective area of radiation. In addition the ratio of narrow-band emission to the broadband background is determined completely by intrinsic physical parameters, the radiative transition probability given by the dipole moment of the subband wavefunctions /19/ and the dynamical conductivity which limits the broadband continuum optical properties of the system. This latter argument also applies for the minigap emission /20/ although the emission from tilted surfaces reaches higher emission intensities (up to some 10^{-10}W/cm^{2}cm^{-1}. For these reasons the main interest was concentrated on the radiative decay of two-dimensional plasmons via periodic grating structures. In these devices the emission intensities can be increased to values over 10^{-8} W/cm^{2}cm^{-1} and the ratio of narrow-band signal to background can be determined by external parameters of the grating coupler. The background can be suppressed by choosing the right parameters for the grating design.

The following scopes of the research were given in the proposal:

- Theoretical understanding of: plasmon excitation
  linewidth
  intensity and radiative decay

- Experimental optimization in: frequency tunability
  linewidth
  emitted power

- Applications: Source for spectroscopy
  Detector testing
  Reference source in FIR astronomy

- Investigation on the possibility of coherent emission

The theoretical and experimental work could clear up the mechanisms of plasmon excitation as a thermal process resulting from the different scattering mechanisms of the heated electron system. The emission experiments can be quantitatively explained by the model of plasmon excitation in thermal equilibrium /21/. The influence of all parameters appearing in the system, namely electron concentration n_s, elastic scattering time τ_m, electron temperature T_e, grating parameters a, t (period a and spacing t), effective mass m* and oxid thickness as well as the dielectric properties of the surrounding media on the emission linewidths and intensities were studied experimentally and theoretically. Thus the main goal of the project - to determine the requirements for applicable sources - could be reached. With the known intensities also the two other applications (detector testing and use as a reference source) could be demonstrated.

The possibility of coherent emission is discussed theoretically and is expected to be realized experimentally in the near future since the requirements on electron mobility and sample homogeneity are presently going to be met by world's best existing technologies for GaAs/AlGaAs heterostructures. In addition to the given aims of the project plasmon emission from GaAs/AlGaAs-structures could be demonstrated for the first time. Furthermore the background emission from Si-MOSFET samples was quantitatively measured and used for determining electron temperatures in two-dimensional systems.

B.1. THEORY

B.1.1. Optical properties of 2D-systems

The optical properties of a two-dimensional carrier system as present in Si-MOS-devices and GaAs-AlGaAs-heterostructures can be obtained from the boundary conditions for electric and magnetic field componants:

$$\vec{E}_I + \vec{E}_R = \vec{E}_T \quad \text{and} \quad \vec{n} \times (\vec{H}_I + \vec{H}_R - \vec{H}_T) = \vec{j}$$

(I ... incident, R ... reflected, T ... transmitted, $\vec{n}$ ... normal vector, $\vec{j}$ ... sheet current density).
Using $\vec{j} = \hat{\sigma}(\omega)\vec{E}_T$ ($\hat{\sigma}(\omega)$ ... dynamical conductivity of the 2D-system one obtains for the absorption A

$$A = \frac{4Re\hat{F}}{[1 + \sqrt{\varepsilon_s} + \hat{F}]^2}$$

where $\hat{F} = (\hat{\sigma}(\omega) + \hat{\sigma}_{Gate}(\omega))/c\varepsilon_o$ and ε_s is the dielectric constant of the semiconductor substrate.

The dynamical conductivity $\hat{\sigma}(\omega)$ is well approximated by the Drude form

$$\hat{\sigma}(\omega) = \frac{n_s e^2 \tau}{m^*(1 - i\omega\tau)}$$

as it has been shown by FIR and microwave transmission experiments by Allen et al. /22/. In the case of a not spatially homogeneous system, however, the dynamical conductivity has to be modified into $\hat{\sigma}(\omega, \vec{k})$, which will give rise to two-dimensional plasmon phenomena.

B.1.2. The dynamical conductivity $\hat{\sigma}(\omega, \vec{k})$ in two dimensions

The dynamical conductivity $\hat{\sigma}(\omega, \vec{k})$ as a function of frequency and wave vector can be calculated from the response of a 2D-electron system to an external electric field $\vec{E}(\omega, \vec{k}) = \vec{E}_o(\omega, \vec{k})e^{i(kx - \omega t)}$. The 2D-system is screened by a metallic

gate at distance d. Solving Poisson equation in conjunction with the continuity equation gives in the electrostatic limit /23/

$$\hat{\sigma}(\omega, \vec{k}) = \frac{\hat{\sigma}(\omega)}{1 - \frac{\hat{\sigma}(\omega)}{i\omega} \frac{k}{\varepsilon_o(\varepsilon_s + \varepsilon_{ox}\coth(k \cdot d))}} \quad .$$

Figure 6 shows $\hat{\sigma}(\omega, \vec{k})$ and $\hat{\sigma}(\omega)$ for two values of τ and typical numerical values of Si-MOS-inversion layers. The k-value chosen is $2 \cdot 10^6 m^{-1}$ corresponding to a period of a = 3 µm ($k = 2\pi/a$). The resonance of $\hat{\sigma}(\omega, \vec{k})$ at $\omega \sim 7 \cdot 10^{12} s^{-1}$ is the <u>two-dimensional plasmon</u>. The dispersion relation of the 2D-plasmon can be obtained explicitly from $\hat{\sigma}(\omega, \vec{k})$ with $\tau \to \infty$:

$$\omega^2 = \frac{n_s e^2}{m^* \varepsilon_o} \frac{k}{\varepsilon_s + \varepsilon_{ox}\coth(k \cdot d)} \quad .$$

Thus ω^2 is proportional to k and the electronic concentration n_s as shown in Fig. 7. Furthermore for small distances of the gate electrode the plasmon is screened and ω is shifted to lower frequencies. At k = 0 (corresponding to a homogeneous electric field) the plasma frequency is zero. No plasmons can therefore be excited in a two-dimensional system by a plane homogeneous electromagnetic wave.

B.1.3. Coupling plasmon - photon

Plasmons $\omega(\vec{k})$ can be excited by an incident electromagnetic wave, if the electric field component in the plane of the 2D-system is spatially modulated with Fourier components $\vec{k}$. This is experimentally verified by using a FIR-transparent gate-electrode (e.g.: 50 Å Ti) with a one-dimensional line-grating of metallic conductivity on top (e.g.: 1000 Å Al)

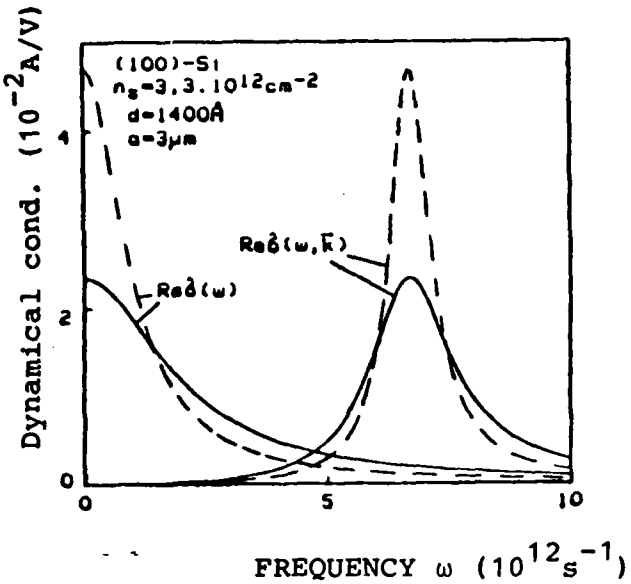

Fig.6: Dynamical conductivities $\hat{\sigma}(\omega)$ and $\hat{\sigma}(\omega,k)$ as a function of frequency for two values of τ (———— τ= 0.5x10^{-12}s, ------ τ= 1x10^{-12} s).

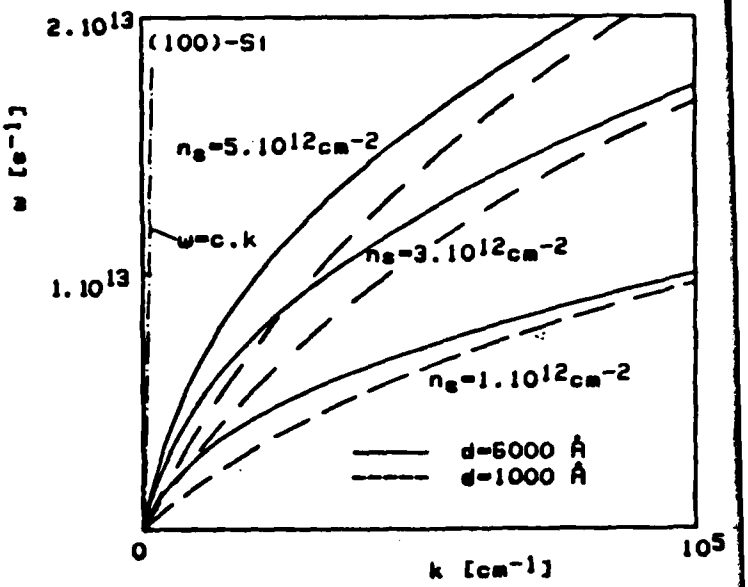

Fig.7: Dispersion relation of the two-dimensional plasmon in (100)-Si for typical values of the carrier concentration and oxide thickness.

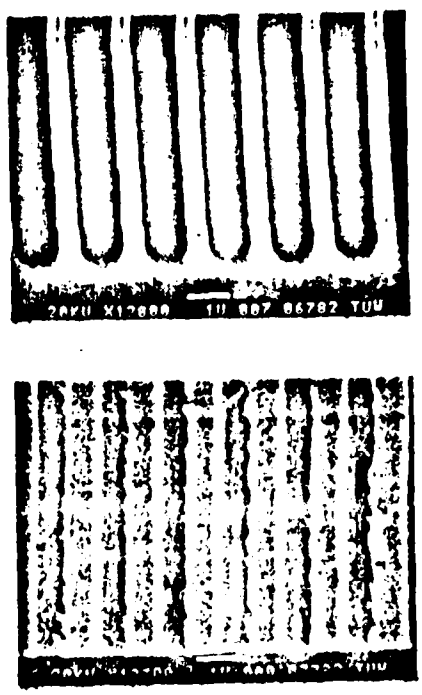

Fig.8: Scanning electron microscopy of a 1.5 µm periodic grating structure. Photoresist structure (above) and final floated Al-structure (below).

with the proper periodicities (1 - 3 μm). Thus the spatially periodic electric field drives currents in the 2D-system due to the high dynamical conductivity $\hat{\sigma}(\omega, \vec{k})$, leading to increased absorption of FIR radiation.

In the particle picture of incident photon and excited plasmon, the grating exchanges the momentum $\hbar k = n2\pi/a$ (a ... grating periodicity) so that momentum conservation is fulfilled if $\hbar \cdot k_{photon} \cdot \sin\gamma \pm 2\pi/a = \hbar \cdot k_{plasmon}$.

Since in the FIR-range $k_{photon} << k_{plasmon}$, the coupling condition turns to

$$\hbar k_{plasmon} = \pm n\, 2\pi/a.$$

The strength of the absorption, quantitatively, depends on the strength of the Fourier components of the electric field at the 2D-system, at the distance d off the grating, which has a periodicity a and spacings of length t. The electrodynamic calculations of the Fourier-components were performed in the linear approximation by Allen et al. /24/ and Theis et al. /25/ resulting in a ratio of the Fourier components with wave vector k_n to the incident wave-field (squared)

$$\alpha_n = \frac{2\sin^2(k_n t/2)}{(k_n t/2)^2} \left[\frac{\sigma_M - \sigma_G}{\sigma_M + \sigma_G(a/t - 1)}\right]^2 \cdot \frac{\coth^2(k_n d) - 1}{\left[\varepsilon_s/\varepsilon_{ox} + \coth(k_n d)\right]^2}$$

(σ_M, σ_G ... sheet conductivities of metal grating and gate, respectively). The absorption of the system thus is given by

$$A(\omega) = \left[\frac{\mathrm{Re}\hat{\sigma}(\omega)}{\varepsilon_o c} + \sum_{n=1}^{\infty} \alpha_n \frac{\mathrm{Re}\hat{\sigma}(\omega, k_n)}{\varepsilon_o c}\right] \cdot \frac{4}{(\sqrt{\varepsilon_s} + 1)^2},$$

which has been confirmed quantitatively by the experiments of Allen et al. /24/ and Theis et al. /25/.

B.1.4. Far-infrared emission

In the following the FIR emission from a 2D-system in which electrons and plasmons are in thermodynamic equilibrium is calculated.

The conditions for a thermodynamic equilibrium in the system are the following:

- Electron temperature: The inelastic electron-electron scattering processes in the system must be much faster than the electron-phonon scattering dissipating energy out of the 2D electron system. This condition is well fulfilled in Si-MOS-systems at low temperatures so that one can use the electron temperature model for describing the energy distribution of the electrons in the electric field: $\tau_{in} \sim 10^{-11}$s, $\tau_e \sim 10^{-9}$s /26,27/.

- Electron-plasmon interaction: There is no direct excitation of one electron to one plasmon, since the 2D plasmon dispersion $\omega(k)$ does not cross the range of possible excitations by single particles given by

$$0 \leq \hbar\omega \leq \hbar^2[k_F^2 - (k_F - k)^2]/2m^* \ .$$

  In the various scattering mechanisms present in the 2D-system (Coulomb-, electron-electron-, surface-roughness, even acoustic-phonon-scattering), the momenta are exchanged properly allowing the excitation of plasmons by an inelastic scattering process /28/. If these plasmon excitation and annihilation processes are much faster than the dissipative processes (radiative decay, plasmon-phonon-scattering), then thermodynamic equilibrium will also exist for the collective excitation. The amount of the plasmon excitation in a hot electron system will thus be given by the appropriate quantum statistics /21/.

In the course of the project it could be shown that also the second condition is fulfilled in Si-MOS-structures and thus

the plasmon excitation can be quantitatively described by a THERMAL excitation model /21/.

The spectral intensity of FIR-emission from a system in thermal equilibrium is given by

$$I(\omega, T)d\omega = \frac{\hbar\omega^3}{4\pi^3 \cdot c^2 \left[e^{\hbar\omega/k_B T} - 1\right]} \cdot A(\omega)d\omega$$

($I(\omega, T)$ ... spectral emission intensity per solid angle per unit area, $A(\omega)$ ... spectral absorptivity).
Regarding only the first Fourier component $A(\omega)$ is given by

$$A(\omega) = \left[\frac{\mathrm{Re}\hat{\sigma}(\omega)}{\varepsilon_o c} + \alpha \frac{\mathrm{Re}\hat{\sigma}(\omega, \vec{k})}{\varepsilon_o c}\right] \frac{4}{(\sqrt{\varepsilon_s} + 1)^2} \quad .$$

Thus the FIR emission consists of two parts, a broadband spectrum from hot-electron emission described by $\hat{\sigma}(\omega)$ and a narrowband peak from the radiative decay of two-dimensional plasmons ($\hat{\sigma}(\omega, k)$).

The narrowband peak should increase with

- increasing electron concentration n_s
- increasing lifetime $\tau_{plasmon}$
- increasing electron temperature
- increasing coupling parameter α.

In our experiments all these dependencies including the linewidth behaviour were studied systematically and could prove the theoretical models. Some numerical data for strong FIR sources will be given in section B.3.1.

B.2. EXPERIMENTS

B.2.1. Technological

Starting-point for the production of plasmon emission devices were large Si-MOSFETs on (100)-Si-surfaces (gate area 2.5 x 2.5 mm^2), produced at Bell Laboratories, Murray Hill, NJ, by G. Kamminsky. The oxide thickness of the samples is between 1000 and 6000 Å, the peak mobilities are between 5000 and 15000 cm^2/Vs.

The aim was the fabrication of high quality metal gratings with periodicities of 5 µm, 3 µm and smaller periods on an area of at least 1.5 x 1.5 mm^2. The lines were first cut out of a "Rubilith"-foil (two layer foil) as 1 mm/1 mm structures by a computer-controlled "coragraph" cutting machine using a loop program.

Then the foil was reduced 40 times (5 µm-grating) and 66 times (3 µm) by photographing it on a gelatine mask (KODAK HR plates). The mask was then copied on an Fe_2O_3-mask covered with 0.2 - 0.3 µm AZ 1300 photo-resist. The Fe_2O_3-mask was etched and afterwards reduced to the final Fe_2O_3-mask by microprojection with a fixed reduction factor of 10. The results of these procedures were masks with grating-periodicities of 5 µm on an area of 1.75 x 1.75 mm^2 and 3 µm on an area of 1.05 x 1.05 mm^2. Different ratios of the grating-width to spacing were obtained by varying the exposing times of the microprojection. The Au-Gate of the MOS was etched away (using 400g KI, 100g I_2, 400ml H_2O) so that only the transparent Ti-Gate remains. After careful cleaning (hot Tri, Aceton, Methanol) the Ti-surface is treated shortly with HMDS (= 1,1,1,3,3,3 Hexamethyl-disilazan) which causes a better adhesion of the photoresist.

The samples (Si-MOSFETs and GaAs-AlGaAs-heterostructures) were coated with Shipley AZ 1350J photoresist of ∿1.5 µm thickness. After baking at 90°C for 20 minutes the photoresist was

exposed for 8 seconds on the Süss-MJB3-contact lithography machine. To obtain grating structures on larger areas than 1.05 x 1.05 mm^2 (3 µm periodicity) the exposing was repeated up to 4 times using shorter exposing times (6 sec.). It was possible to fabricate up to 4 mm^2 of high quality 3 µm-gratings.

The final process was the evaporation of Aluminium (1000 Å) and the lifting-off of the photoresist with the deposited Aluminium by floating in a bath of Ketone to obtain the Al-grating-structure on the samples.

The technological work was improved by using e^--beam-exposed and plasma-etched Cr-masks on quartz (purchased from VALVO, Germany) with periods of 2 µm, 1.5 µm and 1.0 µm. We could fabricate Al gratings with 1.5 µm - periods on Si-MOSFETs and GaAs-samples by optical contact lithography and lift-off metallization. Fig. 8 shows SEM-photographs of samples with 1.5 µm - periodic gratings. We also produced samples with sinusoidall semitransparent metal gratings, without "lifting-off" the stripes. The emission experiments (plasmon as well magneto-plasmon studies) demonstrate the possibility of using "non-lifted", only rectangularly or sinusoidally corrugated metallic gratings as antennas, which allow smaller grating constants by holographic methods. The necessarity of lift-off for a long time limited the production of finer gratings.

In the final periods of the project a holographic exposure system has been built up in order to make gratings of 0.8 to 0.2 µm period /29/. The interfermometric arrangement for producing relief patterns is shown in the figure below. A beam splitter devides the radiation of a HeCd-laser (3250 Å, ∿10 mW) into two beams that are superimposed at an angle 2 Θ to form an interference pattern in the photoresist. The spatial filters consist of 10x quartz UV objective lenses and 3 µm pinholes and provide the beam expansion and smoothing of the intensity profile. The final collimating lenses can be omitted, since also spherical coherent waves from the pinholes produce a linear grating pattern in the central region. By varying Θ the period of the grating can be changed.

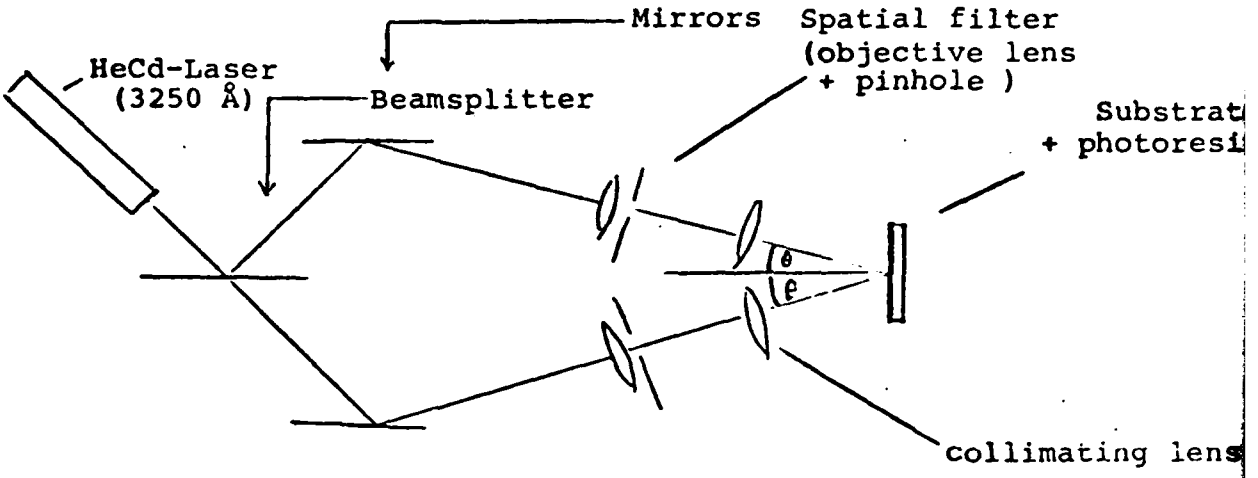

Fig.9: Experimental arrangement for interferometric exposure of the photoresist.

B.2.2. FIR-emission experiments

Detectors

For the analysis of the FIR emission high-purity-n-GaAs detectors were used which have a maximum in the photo-conductivity (fig.4) at $\tilde{\nu} = 35.5\ cm^{-1}$ due to the 1s - 2p - impurity transition /30/. The detectors are tunable with a magnetic field B, which splits up the transition into three lines, and can be used up to $80\ cm^{-1}$. At B = 0 the responsivity of the whole detector arrangement was measured to be $4 \cdot 10^{6}$ V/W at constant $I_D = 2 \cdot 10^{-9}$A, the noise equivalent power $5 \cdot 10^{-14}$ W/$\sqrt{Hz}$.

Emission set-up

Figure 10 shows the experimental arrangement used for the emission work. On both ends of a polished brass-waveguide the emitting MOS device and the detector are mounted. Waveguide and sample holders are immersed in liquid helium.

During the experiment the gate voltage is tuned which changes the electron concentration and thus the frequency of the plasmon corresponding to a certain wave vector fixed by the grating

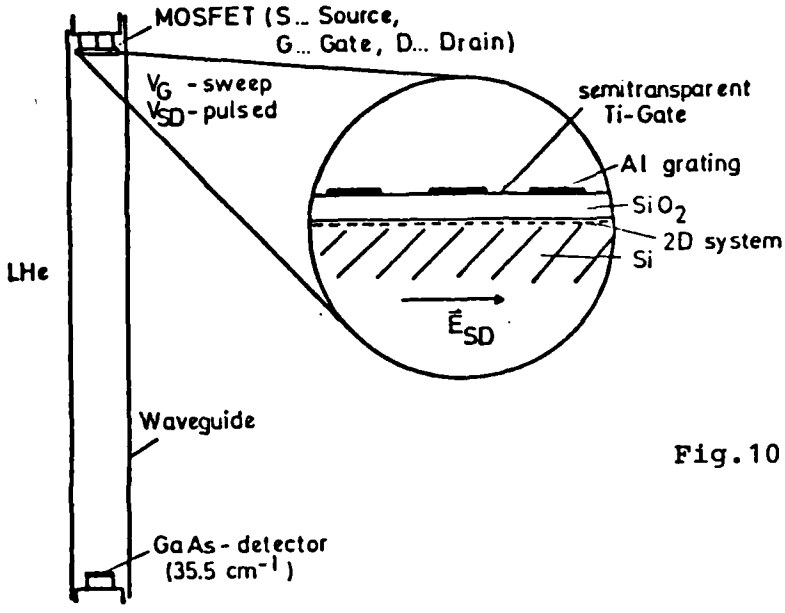

Fig.10: Experimental set-up for FIR emission experiments and cross-section of the MOSFET-sample with plasmon-photon grating coupler.

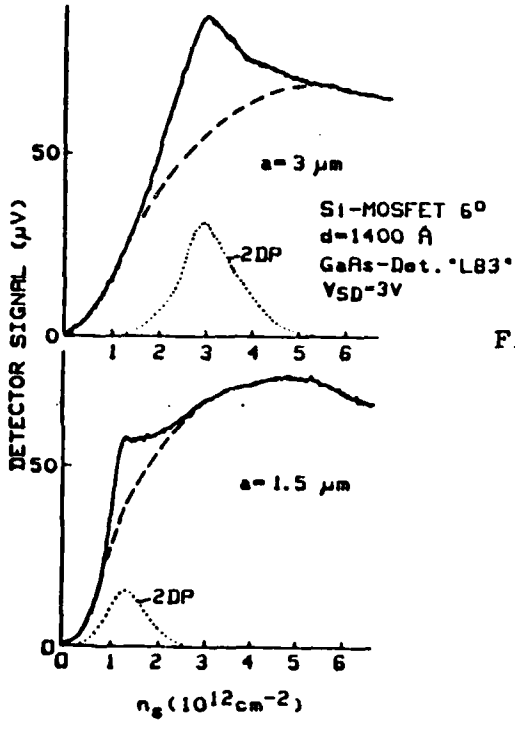

Fig.11: FIR-emission at 35.5 cm^{-1} of sample B6° with different grating structures (above: a = 3 μm, below: a = 1.5 μm).

periodicity. Between source and drain pulses of 0.5 to 50 V are applied (0.1 to 3 ms) in order to heat up the electron system. The periodic detector signals are measured with Lock-In-technique. Superconducting coils (up to 8 T) allow plasmon experiments in the magnetic field (magneto-plasmon studies) and tuning of the detector.

Results

Figure 11 shows a typical plot of the detector signal as a function of the electron concentration for two different values of the grating wavevector (periodicities 1.5 µm and 3 µm). Superimposed on the broadband FIR emission (dashed curves) by hot electron emission (see B.3.4.) a narrowband signal due to radiative decay of two-dimensional plasmons is observed. The n_s-position depends on the grating wavevector and the detector's resonant frequency (here 35.5 cm^{-1}). Tuning the detector by a magnetic field B_D allow the comparison of the narrowband signal with the plasmon dispersion. This is shown in fig. 12 for a = 1.5 µm: The agreement of the resonant positions leaves no doubts on the origin of the resonance as two-dimensional plasmon excitation. The dependence of the n_s-position for $\tilde{\nu} = 35.5 cm^{-1}$ ($B_D = 0$) on the grating wave vector and oxide thickness is shown in fig.13 resulting in the same agreement of experiment and theory.

In order to clear up the mechanism of excitation of the two-dimensional plasmon by the source-drain-current, the experiments were performed using different orientations of the grating wavevector in respect to the source-drain-field direction respectively current direction. The results of this experiments are shown in figure 14. The narrowband emission is absolutely independent of the orientation of the grating in respect to the current direction. This result excludes the possibility of the drift of the electron gas along the grating playing a role for the excitation, as it would be the case in free-electron effects (Smith-Purcell effect, travelling-wave

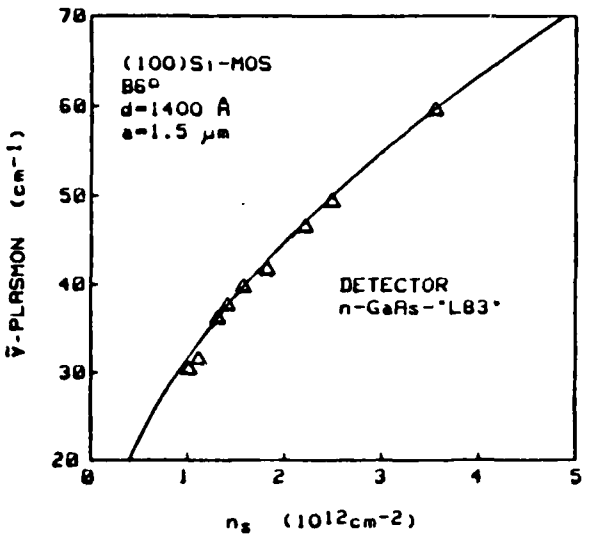

Fig.12: Comparison of the experimentally measured frequencies of the 2D-plasmon (a = 1.5µm) and theoretical dispersion relation.

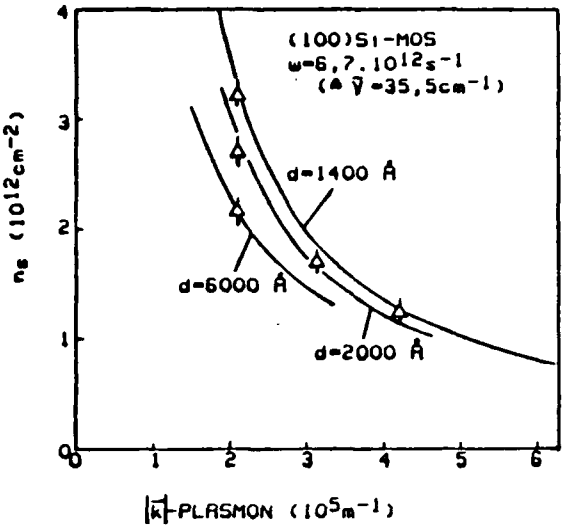

Fig.13: Theoretical and experimental values of n_s as a function of plasmon wavevector and oxide thickness at the detector frequency of 35.5 cm^{-1}.

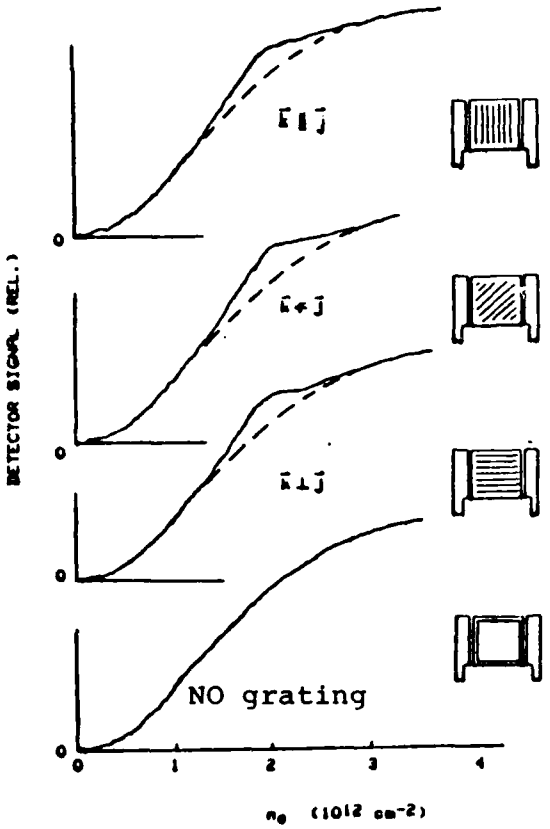

Fig.14: FIR emission of MOSFET B9/9 (a=3µm, d=6000 Å, V_{SD}=3V) at 35.5 cm^{-1} with different grating orientations and without grating.

tubes, etc.). The quantitative agreement with the theory of thermal excitation will give the evidence of a thermal excitation mechanism by Coulomb scattering in the system.

Linewidths

The linewidth of the emission is mainly determined by the single particle scattering mechanisms. This can be seen in figure 15, where a comparison of the plasmon lifetime (obtained from the experimental linewidth) and the single particle momentum relaxation time is made: The plasmon lifetime is always somewhat smaller than the single particle relaxation time. This indicates that, in addition to the damping mechanism by single particle scattering, electron-electron-scattering ($\sim 10^{-11}$s) as well as the radiative decay slightly damp the plasmon excitation. The scattering mechanisms thus are found to dominate the linewidth: A sharp emission line is therefore only possible in systems with high mobility (GaAs-AlGaAs-heterostructures, see B.5.)

Intensities

Absolute intensities of the radiation could be determined by comparison with InSb cyclotron emission /31/ at saturation electron temperatures, which is around 40 K at a magnetic field of 0.6 T /32/ giving a maximum cyclotron emission intensity of $\sim 3 \times 10^{-8} W/cm^{-2}$ within the GaAs-detector interval of 2 cm^{-1} (at $B_D = 0$).

In figure 11 the peak emission intensity of the narrowband peak is plotted versus the electron temperature of the inversion layer. The emission is detectable from 10^{-13}W on and increases up to $10^{-9} W/cm^{-2}$. The experimental data agree in absolute values with the theory of thermal plasmon excitation. The sample with a = 3 µm (□) has a higher intensity due to better coupling ($k \cdot d$ smaller) and higher dynamical conductivity (higher n_s). Of course the experimental data are always somewhat below the theory since imperfections in the gratings slightly reduce the emission intensity.

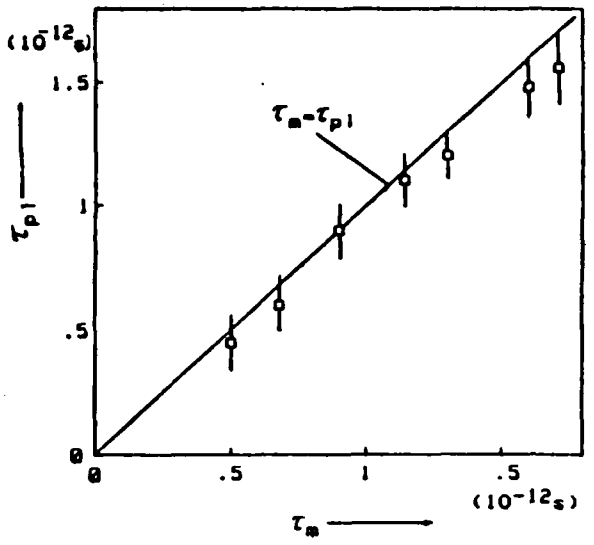

Fig.15: Relaxation time of the two-dimensional plasmon (from the linewidth of FIR emission) in comparison to the momentum relaxation time τ_m of the single electron (from transport measurements).

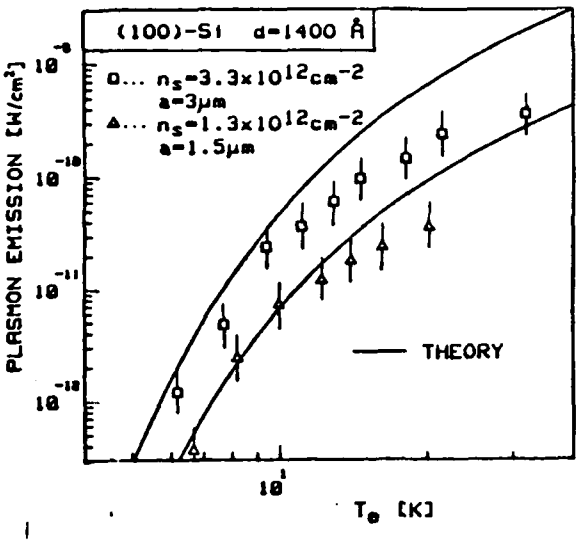

Fig.16: Intensity of plasmon emission within the detector interval of 2 cm^{-1} as a function of the electron temperature T_e.

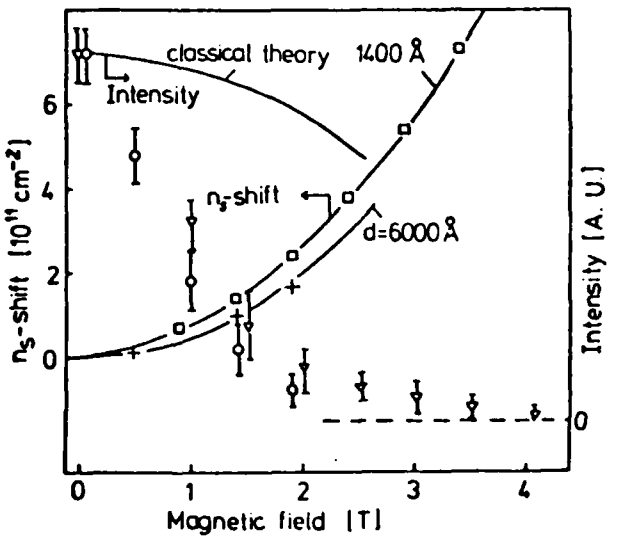

Fig.17: n_s-positions and intensity behaviour of plasmon emission in the magnetic field for two different samples.

From long series of measurements it is found that the theory of thermal excitation can quantitatively explain all experiments performed and thus the performance of the plasmon sources can be discussed on the basis of this theory. In section B.3.1. this discussion will be made in the view of the optimization of the emission source.

Magnetoplasmons

An additional possibility of tuning the frequency of plasmon-emission is the "magnetoplasma"-effect which was seen for the first time in emission in the course of this project by Höpfel et al. /28/. In figure 17 the n_s-shift of the resonance at 35.5 cm^{-1} is plotted as the magnetic field: This behaviour accurately follows the theory /33/ simply expressed by

$$\omega_{mp}^2 = \omega_p^2 + \omega_c^2$$

ω_c ... cyclotron frequency
ω_p ... plasmon frequency
ω_{mp} ... magnetoplasmon frequency

The intensity of the radiation, however, strongly decreases, much stronger than expected from the dynamical conductivity /25/ as it can be seen in figure 17. This decrease is due to inhomogeneous heating in the Hall field at the edge of the inversion layer and also to Landau-damping mechanisms that become possible by the additional states in the $E(\vec{k})$-space that are induced by the magnetic field.

B.3. APPLICATIONS

B.3.1. Tunable FIR sources

The evidence of thermal plasma excitation and the quantitative agreement of the experimental FIR emission with theory allows a detailed discussion of the FIR emission as a function of all parameters.

Electron concentration n_s

The higher n_s the higher is the dynamical conductivity $\hat{\sigma}(\omega, \vec{k})$. Thus a high electron concentration increases the emissivity of the system. The mobility of the electrons, however, decreases for $n > 1 \times 10^{12} cm^{-2}$ due to oxide roughness scattering. Thus the linewidth of the narrowband emission increases at high electron concentrations.

Grating periodicity

The grating periodicity mainly determines the range of tunability of the source. Since the best results in Si-MOSFETs were obtained in the electron concentration range of $0.8 \leq n_s \leq 4 \times 10^{12} cm^{-2}$, the following tuning ranges can be specified:

grating periodicity	$\omega(10^{12} s^{-1})$	$\tilde{\nu}(cm^{-1})$
1 µm	6 - 16	32 - 85
3 µm	4 - 10	21 - 59
5 µm	2.5- 7	13 - 37

The linewidth is not affected directly by the grating periodicity, whereas the intensity of the emission depends via the coupling parameter α strongly on the grating periodicity: The coupling efficiency decreases with higher wave vectors, since the strength of the Fourier components is decreasing with e^{-2kd}

where d is the oxide thickness. Therefore the oxide thickness should be reduced in the same scale as the grating periodicity in order to obtain efficient coupling constants also at high wave vectors.

Grating design

Our experiments as well as the electrodynamical calculations performed by Theis /25/ as well as Allen et al. /24/ give evidence that for an efficient coupling it is both necessary that the oxide thickness is as small as possible and that the grating spacings t are small compared to the grating period a to give a maximum value of the coupling constant α. This is mainly a technological problem to make thin oxides (< 1000 Å) without defects and to optimize photolithography for thin grating spacings t. In our samples we could reach values of α of up to 0.21 (d = 1400 Å, a = 3 µm, t/a = 0.5) whereas the ideal value ($d \to 0$, $t/a \to 0$) would be 2. So there is still an order of magnitude to increase the efficiency (and the peak-to-broad-band emission ratio) to improve, if thinner oxides would be used, especially.

Electron temperatures

The electron temperatures are the limiting parameters for the emission intensities in the thermal equilibrium via Bose-Statistics of plasmons and photons. In the thermal equilibrium the emission intensity cannot exceed the values given by Planck's radiation law. This means that for typical electron temperatures that can be achieved in Si-MOSFETs the following emission intensities (per frequency interval, per solid angle, per cm^2 source area) can be reached. One polarisation direction due to the grating coupler, a factor of 0.5 in addition always limits the emissivity of a two-dimensional system due to the boundary conditions of the tangential component of the electric field.

$\tilde{\nu} = 35.5\ cm^{-1}$

T_e	max.emission intensity (W/cm^2cm^{-1})	experimentally achieved intensity (W/cm^2cm^{-1})
4.2	2×10^{-13}	---
10	2×10^{-10}	2.5×10^{-11}
15	1×10^{-9}	1×10^{-10}
20	3×10^{-9}	3×10^{-10}
25	7×10^{-9}	5×10^{-10}
30	1×10^{-8}	6×10^{-10}
40	2×10^{-8}	8×10^{-10}
50	3×10^{-8}	$\sim 10^{-9}$
100	1×10^{-7}	---

For higher electron temperatures high electric source-drain fields have to be applied. This brings problems due to the "pinch-off"-effects: The source-drain-voltage becomes comparable to the gate voltage which leads to an inhomogeneous electron concentration in the 2D-system, and, as a consequence of the inhomogeneous conductivity, to a highly inhomogeneous electron temperature.

In order to overcome this problem, we applied already at moderate field (10 - 25 Vcm^{-1}), a d.c. "compensation voltage" along the transparent gate electrode to provide a homogeneous gate potential along the whole length of the inversion channel (see fig. 18). At source-drain-fields larger than 25 Vcm^{-1}, the gate itself starts strongly emitting FIR-radiation, which limited the experiments with "compensation voltage" to fields of about 25 Vcm^{-1}.

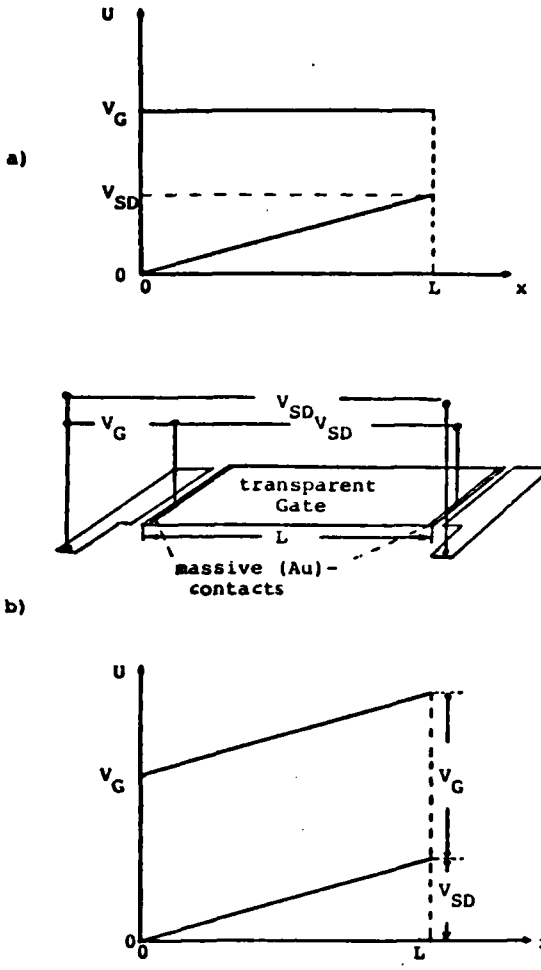

Fig.18: a) Gate-channel-potential along the length L of the inversion channel,

b) experimental scheme of the "compensation-voltage"-method (above) and potential along the channel at compensation voltage V_{SD}.

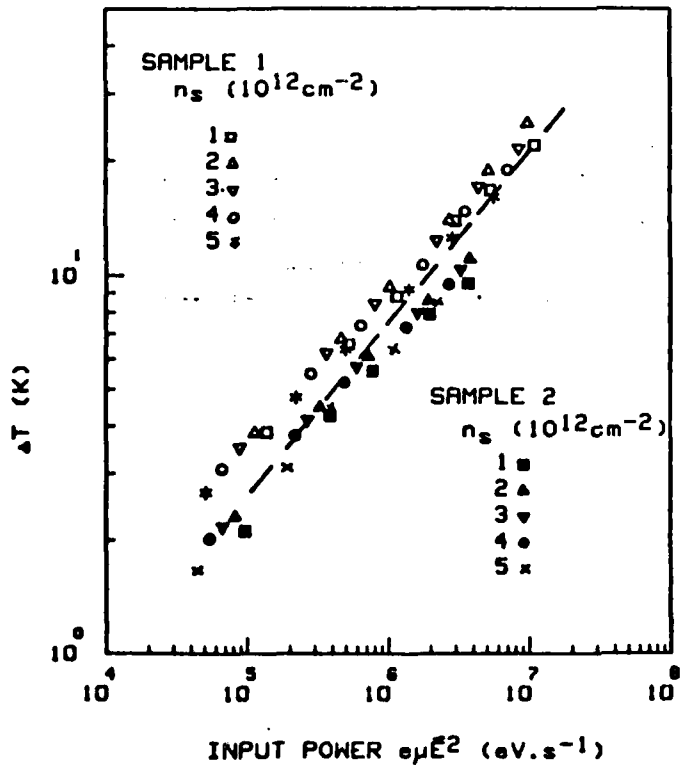

Fig.19: Electron temperatures in the Si-inversion channel as a function of the input power per electron $e\mu E^2$ for two different types of samples (1...high mobility, 2 ... low mobility).

Linewidths

As reported in B.2.2. the linewidth is correlated with the elastic scattering time τ_m of the single particles. This is experimentally manifested in linewidths that are - depending on the mobility - between 3.5 and 7 cm^{-1}. The sharpest lines were observed with a MOSFET having μ_{peak} = 18.000 cm^2/Vs at $n_s = 1.0 \times 10^{12} cm^{-2}$ with a linewidth of 3.0 cm^{-1}.

The scattering process not only limit the linewidth but also the intensity via the dynamical conductivity and increase the background broadband emission from hot electrons. Therefore it is necessary for applicable devices to use systems with high carrier mobilities. Si-MOSFETs are physically limited to $\mu \sim 25.000$ cm^2/Vs, the well-known modulation doped GaAs/AlGaAs-heterostructures, however, reveal mobilities exceeding $10^6 cm^2/Vs$ and are therefore predestinated for narrowband sources, if the FET-technology is developped furthermore (see section B.5.).

B.3.2. Detector testing - reference sources

Although the emission intensities and especially linewidths of the Si-MOS-emission sources cannot compete with magnetically tunable sources (see section A), the emission by two-dimensional systems offer a variety of applications as reference sources of well-known absolute intensities. The absolute emission intensity of a 2D-source of known electron temperature is accurately given by the theory (see section B.1.4.). The advantages to bulk semiconductor samples are the following: The electron concentration values and scattering times - that determine the optical properties of the system - are well measurable by transport and Shubnikov-de Haas measurements. No problems with FIR-emitting contacts arise. The electric field which heats up the electron system is known and not modified by magnetic inductions as it is the case in magnetically tunable devices. The electron temperature is a known function of the electric field (see next

section) independent of effective mass, g-factor and, especially, the electron concentration n_s, as it has been shown theoretically and experimentally by our group recently /34,35/.

Therefore 2D-systems are - for broadband as well as narrowband emission - sources with highly reproducible and well-known emission intensities for use as reference sources (power levels 10^{-14} - 10^{-9}W) as well as for testing sensitive detectors in the FIR-range.

B.3.3. Electron temperature measurements

FIR emission from the inversion layer of the Si-MOSFETs brings a new method of determining electron temperatures. Since the broadband FIR absorption by the 2D electron system is known experimentally /22/ and theoretically (B.1.4.), the absolute emission intensity of FIR-radiation from the 2D electron system represents a direct measure for the electron temperature T_e.

In these experiments we used MOSFETs with transparent gate electrodes and a GaAs-detector, whose responsivity at 35.5 cm^{-1} has been determined accurately by using a Carbonglass-bolometer as a reference source; in addition the absolute intensity is determined by comparison with InSb-cyclotron emission at saturation electron temperature. The 2D electron system is heated by applying electric source-drain pulses of 0.5 V up to 10 V to the MOSFETs. Simultaneously the current-voltage characteristics of the MOSFETs is measured to determine the n_s- and field dependent mobilities of the sample for the calculation of the input power $e\mu E^2$ and the dynamical conductivity $\hat{\sigma}(\omega)$.

We investigated MOS-samples with different mobilities from 2.000 up to 10.000 cm^2/Vs. In figure 19 the evaluated electron temperatures are plotted versus the input power $e\mu E_{SD}^2$ which, in equilibrium situation, is equal to the power loss of the

hot electron gas. In the figure also the slope for $\Delta T \propto (e\mu E^2)^{1/2}$ is indicated. As a result the electron heating ΔT is in the whole range of temperature exactly proportional to the square root of the input power respectively the power loss $e\mu E^2$. We can therefore express the electron heating as a function of the input power $e\mu E^2$ quantitatively as

$$\frac{\Delta T}{(e\mu E^2)^{1/2}} = (0.7 \pm 0.2) \cdot 10^{-2} K\ s^{1/2}\ (eV)^{-1/2} \quad .$$

These values are lower than the electron temperatures obtained at low electric fields by Fang and Fowler /36/, Kawaji and Kawaguchi /37/ and Hönlein and Landwehr /38/, but fairly agree with the values obtained from subband emission /27/. FIR-emission is the first method that can give results in the whole temperature range of 2 K up to more than 30 K. The linear dependence of ΔT on $(e\mu E^2)^{1/2}$ is predicted by recent theories of acoustic phonon scattering in 2D systems /35,39/ up to electron temperatures of at least 50 K.

With the method of FIR-broadband-emission we were furthermore able to measure the effect of increased carrier heating /34,38/, when a negative substrate bias is applied. The effect is due to a decreased channel width and an influence of SiO_2 phonon modes /38/.

B.4. COHERENT EMISSION

The generation of radiation by radiative decay of plasmon oscillations in semiconductors is a quite new phenomenon. At present only spontaneous emission has been observed since the plasmon lifetimes are too short to enable an efficient interaction with the grating. In systems with high electron concentrations it was found that the excitation can be described with an electron temperature distribution, that means as a quasi-thermal process. The plasmon lifetimes are similar to the momentum scattering time in the order of 10^{-12}s. The radiative decay time of the plasmons induced by the grating is several orders of magnitude longer than the nonradiative lifetime ($\tau_{rad} \sim 10^{-7} - 10^{-8}$s). However, in Si-MOSFETs the observed τ_{rad} was found to be shorter than for any other radiative quantum transition in the system /21/. An increase of the emitted intensity can only be achieved if the system can be driven out of the thermal equilibrium with the single electron excitations.

One way to achieve this is to obtain such a strong coupling between grating and two-dimensional electron gas, so that the grating influences the plasma wave generation process. One of the drawbacks of the system is that a continuous plasmon spectrum is excited by the current generation process. The generation process is not effective since only one single mode is coupled out by the grating. If the grating influences the generation process a higher density of plasmons with the proper wave vector is generated. This would lead to a higher emission intensity. However, in this case the distribution has to be a non-thermal one to prevent a thermalization of the selective excitation. The requirements for this process are that the plasmon wave extends over a large number of grating periods and that the plasmon lifetime is dominated by the radiative

decay time induced by the grating. In semiconductors as Si and GaAs the requirements would be met with optimized gratings (high α) and mobilities in the order of $10^6 cm^2/Vs$. For Si this is not realistic but in GaAs mobilities for two-dimensional electron systems up to $1.5 \times 10^6 cm^2/Vs$ have been obtained recently.

Another way to obtain stimulated emission is analogous to the backward-wave oscillator. If the drift velocity of the carrier gas is equal to the phase velocity of a certain plasmon mode a direct conversion of drift energy into a plasmon oscillation with a fixed wavevector is possible. This system would not require a grating structure for spontaneous emission (while in the case $v_{drift} < v_{ph}$ a grating is necessary even for spontaneous emission): The plasmon mode with $v_{ph} = -v_{drift}$ already fulfills the coupling condition without a grating: The plasma wave in the drifting system represents an oscillating charge density that is able to radiate. For the stimulated excitation a grating would be necessary in order to amplify the spontaneous density modulations coherently, but also other methods of feedback (e.g. resonant cavities) are possible. The coupling to all other excitations of the system which are not in resonance with the drift of the carriers will be weaker. The phase velocities of plasma waves in inversion channels of GaAs/GaAl As structures range from a few $10^7 cm/s$ to $10^8 cm/s$. A drift velocity of $3 \times 10^7 cm/s$ (equal to the saturation velocity in high fields) can be achieved in samples with a mobility of $1.5 \times 10^6 cm^2/Vs$ /40 /. Since these mobilities can be achieved in GaAs/GaAlAs heterostructures a stimulated emission from plasmon waves in semiconductors seems possible. However, a serious drawback can be the interactions of the plasmon wave with the single electron excitations and the lattice phonons which have to be studied in detail in the future.

B.5. PLASMONS IN GaAs/AlGaAs STRUCTURES

In view of the ultra high mobilities that can be achieved in 2D systems in GaAs, we performed plasmon experiments also in this material /41/.

The investigated samples were first low mobility ($\sim 2 \cdot 10^4 cm^2/Vs$) GaAs/AlGaAs heterostructures with a 2D electron gas of a density $n_s = 8.25 \times 10^{11} cm^{-2}$ as determined by Shubnikov-de-Haas oscillation. The electron density can be increased by illumination with band gap radiation to $8.9 \times 10^{11} cm^{-2}$. With a 5 µm-grating placed on top of the AlGaAs, resonant emission was observed at a frequency of 29 cm^{-1} by means of InSb-cyclotron resonance detectors. After replacing the 5 µm-grating by a grating of 3 µm period, the emission has been observed changing according to the dispersion relation.

The radiation intensity observed is in the order of nearly $10^{-8} W$ and thus more than one order of magnitude higher than from Si-MOSFETs. The reasons are better dielectric coupling and higher electron temperatures in these systems.

In samples with high mobilities (up to 300.000 cm^2/Vs) the linewidth was observed to be much smaller ($< 2 cm^{-1}$) but did not reach the expected values, probably because of electron-electron interaction. This generates and annihilates plasmons, but has no influence on the transport properties.

The experiments show generally that plasmons can be excited in GaAs-AlGaAs-heterojunctions. The thin AlGaAs layer ($d \sim 700$ Å) and the dielectric properties give high values of the coupling efficiency and thus higher power levels. If one succeeds in making transparent gates with grating structures the material would also be favourable for electrically tunable sources. The high drift velocities moreover promise striking emission experiments out of the thermal equilibrium for the near future (see B.4.).

References

/1/ E. Gornik in "Lecture Notes in Physics" Vol. 133 (1980) p. 160-175, ed. W. Zawadski, Springer Verlag, and J. of Magnetism and magnetic materials 11 (1979) 39.

/2/ G. Lindemann, W. Seidenbusch, R. Lassnig, E. Gornik, Phys.Rev.B 28 (1983) 4693.

/3/ P.G. Harper, J.W. Hodby, R.A. Stradling, Reports on Progress in Physics 36 (1973) 1.

/4/ G. Lindemann, E. Gornik, R. Schawarz, D.C. Tsui, Inst. Phys.Conf.Ser. Nr. 56, Chapter 8 (1981) 631.

/5/ S. Porowski in "Lecture Notes in Physics" Vol. 152 (1982) p. 420, Springer Verlag.

/6/ E. Gornik, R.A. Höpfel, M. Baj, S.Porowski, Z. Wasilewski, A.M. Davidson, R.A. Stradling to be published.

/7/ V.I. Sheka, Sov.Phys.Solid State 6 (1965) 2470.

/8/ E.I. Rashba and V.I. Sheka, Sov.Phys.Solid State 3 (1961) 1257.

/9/ F. Kuchar, R. Meisels and M.Kriechbaum, Proc. 4th Int. Conf.Phys.Narrow Gap Semicond., Linz, 1981, ed. by E. Gornik (Springer, Berlin 1982) p. 197.

/10/ B.D. Mc Combe, Phys.Rev.B 181 (1969) 1206.

/11/ R.J. Wagner and G.A. Prinz, Appl.Optics 10 (1971) 2060.

/12/ B.D. Mc Combe and R.J. Wagner, Proc. 11th Int.Conf.Phys. Semicond., Warsaw 1972, ed. by M. Miasek (PWN, Warzaw, 1972) p. 321.

/13/ B.D. Mc Combe, Proc.Int.Conf.Appl.High.Magn.Fields Semicond.Phys., Würzburg 1974, p. 146.

/14/ M. Kriechbaum, R. Meisels and F. Kuchar , Proc. 16th Int. Conf.Phys.Semicond., Montpellier 1982, ed. by Averous (North Holland, Amsterdam 1983) p. 444.

/15/ F. Kuchar and M.Kriechbaum, Proc.Int.Conf. Appl.High. Magn.Fields Semicond.Phys., Grenoble 1982, ed. by G. Landwehr (Springer, Berlin 1983) p. 309.

/16/ R. Meisels, Thesis "Spectroskopie an III-V Halbleitern im Fernen Infrarot", University Vienna (1983) F. Kuchar and R. Meisels.

/17/ S. Komiyama, Advances in Phys. 31, Nr. 3 (1982) 255-297.

/18/ E. Gornik, D.C. Tsui, Phys.Rev.Lett. 27 (1971) 925.

/19/ T. Ando, A.B. Fowler, F. Stern, Rev.of Mod.Physics 54 (1982) 437.

/20/ D.C. Tsui, E. Gornik, Appl.Phys.Lett 32 (1978) 365.

/21/ R.A. Höpfel, E. Vass, E. Gornik, Phys.Rev.Lett. 49 (1982) 1667.

/22/ S.J. Allen, D.C. Tsui, F. DeRosa, Phys.Rev.Lett 35 (1975) 1359.

/23/ T.N. Theis, Surface Science 98 (1980) 515.

/24/ S.J. Allen, D.C. Tsui, R.A. Logan, Phys.Rev.Lett. 38 (1977) 980.

/25/ T.N. Theis, J.P. Kotthaus, P.J. Stiles, Solid State Commun. 24 (1977) 273.

/26/ S. Kawaji, Y. Kawaguchi,'Lecture Notes in Physics', Vol. 177 , Springer-Verlag 1983, p. 53, ed. by G. Landwehr.

/27/ E. Gornik, D.C. Tsui, Solid State Electronics 21 (1978) 139.

/28/ R.A. Höpfel, E. Gornik, A.C. Gossard, W. Wiegmann, Proc. 16th Int.Conf. on "The Physics of Semicond.", Montpellier, France 1982, ed. by M. Averous (North Holland, Amsterdam 1983) p. 646.

/29/ L.F. Johnson, G.W. Kammlott, K.A. Ingersoll, Applied Optics 17 (1978) 1165.

/30/ G.E. Stillmann, C.M. Wolfe, J.O. Dimmock, in'Semicond. and Semimetals' (ed. by Willardson-Beer) Vol. 12, Academic Press, New York 1977, p. 169.

/31/ E. Gornik, J.Magn.Mat. 11 (1979) 39.

/32/ W. Müller, F. Kohl, H. Partl, E. Gornik, Solid State Electronics 21 (1978) 235.

/33/ N.J.M. Hornig, M.M. Yildiz, Am.Phys. 97 (1976) 216.

/34/ R.A. Höpfel, E. Vass, E. Gornik, Solid State Commun. (1984, in press).

/35/ E. Vass, R.A. Höpfel, E. Gornik, to be published.

/36/ F.F. Fang, A.B. Fowler, J.Appl.Phys. 41 (1970) 1825.

/37/ S. Kawaji, Y. Kawaguchi, Lecture Notes in Physics 177 (ed. by G. Landwehr), Springer Verlag 1983, p. 53.

/38/ W. Hönlein, G. Landwehr, Surface Sci. 113 (1982) 260.

/39/ Y. Shinba, J. Nakamura, J.Phys.Soc.Jpn. 50 (1981) 114.

/40/ M. Inoue, S. Hiyamizu, M. Inajama, Y. Inuishi, Int. Conf.on 'Solid State Devices', Tokyo 1982.

/41/ R.A. Höpfel, G. Lindemann, E. Gornik, G. Stangl, A.C. Gossard, W. Wiegmann, Surface Sci. 113 (1982) 118.

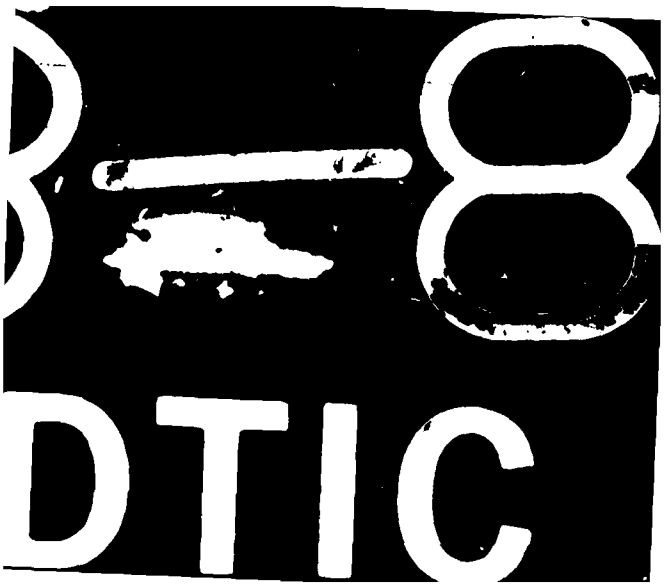
88
DTIC